LETTER

doi:10.1038/nature13262

Storm-induced sea-ice breakup and the implications for ice extent

A. L. Kohout[1], M. J. M. Williams[2], S. M. Dean[2] & M. H. Meylan[3]

The propagation of large, storm-generated waves through sea ice has so far not been measured, limiting our understanding of how ocean waves break sea ice. Without improved knowledge of ice breakup, we are unable to understand recent changes, or predict future changes, in Arctic and Antarctic sea ice. Here we show that storm-generated ocean waves propagating through Antarctic sea ice are able to transport enough energy to break sea ice hundreds of kilometres from the ice edge. Our results, which are based on concurrent observations at multiple locations, establish that large waves break sea ice much farther from the ice edge than would be predicted by the commonly assumed exponential decay[1–3]. We observed the wave height decay to be almost linear for large waves—those with a significant wave height greater than three metres—and to be exponential only for small waves. This implies a more prominent role for large ocean waves in sea-ice breakup and retreat than previously thought. We examine the wider relevance of this by comparing observed Antarctic sea-ice edge positions with changes in modelled significant wave heights for the Southern Ocean between 1997 and 2009, and find that the retreat and expansion of the sea-ice edge correlate with mean significant wave height increases and decreases, respectively. This includes capturing the spatial variability in sea-ice trends found in the Ross and Amundsen–Bellingshausen seas. Climate models fail to capture recent changes in sea ice in both polar regions[4,5]. Our results suggest that the incorporation of explicit or parameterized interactions between ocean waves and sea ice may resolve this problem.

Sea ice is a feature of both polar regions and has an important role in moderating the global climate. The expansion and contraction of sea ice is largely governed by seasonal changes in air temperature, with the finer details controlled by the complex feedbacks that exist between sea ice, the atmosphere and the ocean. Of these feedbacks, the interaction between ocean waves and sea ice is one of the least well understood and is usually overlooked in coupled climate models. Yet the ability of waves to break sea ice has been known since the 'heroic age' of polar exploration[6]. Waves propagating through sea ice leave behind a wake of broken ice floes, which are then more easily deformed by winds and currents, effectively eliminating the barrier between air and ocean and enhancing heat exchange.

The key to predicting the magnitude of ice breakup lies in understanding wave attenuation in the marginal ice zone (MIZ), which is a region, potentially hundreds of kilometres wide, of broken ice floes that forms at the boundary of the open ocean and the sea ice at each pole. Present models of the breakup process either show only moderate agreement with measurements[7], or results are not compared to measured data[8]. Models have typically depended on measurements collected during the 1970s and early 1980s[9,10], in experiments conducted over short timescales and in relatively low-amplitude ocean swells. Large storm waves are routinely found in the Southern Ocean[11] and may be anticipated in an increasingly ice-free Arctic. These drive large-wave events that have occasionally been observed at single locations within the MIZ[12–14], but these observations are insufficient to determine how storm-generated waves propagate through sea ice.

Here we report the measurement of wave attenuation using simultaneous observations across hundreds of kilometres in the Antarctic MIZ, and examine its implications for the recent retreat and expansion of Antarctic sea ice. Five wave sensors were deployed on sea ice between latitudes 60.5° south and 63° south on 23 and 24 September 2012 UTC (Fig. 1). Along the deployment transect, the average ice floe diameter increased steadily from 2–3 m at the ice edge to 10–20 m approximately 200 km from the ice edge. Beyond this, there was an abrupt increase in floe diameter to hundreds of metres (Extended Data Table 1). Ice was estimated from manual shipboard observations to be between 0.5 and 1 m thick and was all first-year ice. The rate at which sea-ice concentration increased with distance from the edge was high relative to the climatological rate for this location (Extended Data Fig. 1). The significant wave heights measured by the sensors include relatively calm conditions and three large-wave events (Extended Data Fig. 2). On 1 October 2012 UTC significant wave heights of 3 m were measured 240 km from the ice edge.

Analysis of wave decay in sea-ice focuses on understanding the evolution of the full wave spectrum propagating through the ice. Linear theory assumes that as a wave propagates through ice, the power at each wavenumber decays without transfer of energy between wave numbers. This implies that the significant wave height, which is proportional to the

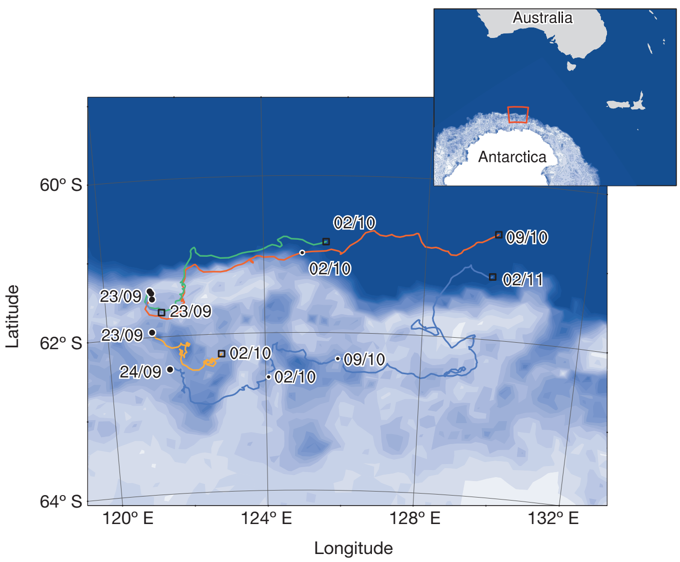

Figure 1 | Deployment location and track of each wave sensor. The large round markers show where and when (day and month UTC) each sensor was deployed. The open square markers show where and when each sensor stopped transmitting. The small round markers indicate the sensor positions on particular dates. Inset, location of the experiment on a larger scale, the red box indicating the main figure. Mean sea-ice concentrations between 23 September and 2 October 2012 are shown with white as 100% sea-ice concentration and blue as open water.

[1]National Institute of Water and Atmospheric Research, Christchurch 8011, New Zealand. [2]National Institute of Water and Atmospheric Research, Wellington 6021, New Zealand. [3]The University of Newcastle, Newcastle, New South Wales 2308, Australia.

square root of the total wave energy, will always decay exponentially with distance from the sea-ice edge[14,15]. Our results confirm previous observations[9,10,16] that, during calm conditions, the significant wave height decays exponentially with distance. However, during three large-wave events, we found that significant wave heights did not decay exponentially, enabling large waves to persist deep into the pack ice.

To demonstrate this, we calculate the decay rate of the significant wave height between wave buoys, dH_s/dx, where H_s is the significant wave height and x the distance between buoys. Using observations farther than 100 km from the ice edge, the magnitude of dH_s/dx increases almost perfectly linearly with H_s until H_s reaches 3 m (Fig. 2). For waves larger than 3 m, dH_s/dx flattens and can be treated as being independent of H_s. This shows that existing linear theory is only valid for waves with $H_s < 3$ m. The empirical model derived from the data is

$$\frac{dH_s}{dx} = \begin{cases} -5.35\times10^{-6}H_s & H_s \le 3 \\ -16.05\times10^{-6} & H_s \ge 3 \end{cases} \quad (1)$$

where -5.35×10^{-6} is the attenuation coefficient. The attenuation coefficients estimated from observations of small waves in the Arctic[10] are also shown in Fig. 2, for comparison. The constant attenuation for waves with significant wave height greater than 3 m implies a more gradual decay of wave height with propagation distance, allowing large waves to penetrate considerably farther into the ice. Because the ice in the MIZ was all first-year ice, we are unable to determine how equation (1) will differ in thicker ice or in a combination of first-year and multi-year ice.

The wave spectra during large-wave events (Extended Data Fig. 3) indicate that the spectral peak of the energy distribution may shift to longer periods with increasing distance from the ice edge. This is standard for waves in the open ocean, where nonlinear interactions create an inverse energy cascade, moving energy and the spectral peak to longer periods[17]. Thus, our observations suggest that nonlinear energy transfer may need to be considered when modelling the decay of large waves ($H_s > 3$ m) through sea ice and that small-amplitude wave theory cannot simply be extrapolated to large-amplitude waves.

We use our new model for wave decay (equation (1)) to estimate the distance from the ice edge over which a wave will be able to break ice floes. Following classical strain theory and using minimum and maximum breaking strains of 3×10^{-5} and 7.05×10^{-5}, respectively[7,8], we consider a wave with a 12-s period travelling through first-year sea ice, and predict ice breaking as a function of significant wave height at the ice edge, assuming that $H \approx H_s/\sqrt{2}$, where H is the single-period wave height (Fig. 3 and Methods). This model can be extended to consider a wave spectrum[8], but the results are almost identical to our single-period analysis. This figure expresses how the wave attenuation that we have observed during large-wave events has a profound impact by transferring energy deep into the ice pack. Also shown are two known observations of ice floe breakup events. One occurred during this experiment (in the Antarctic) and the other occurred in the Arctic[18]. Each observation is a minimum bound on the distance the ice broke during the respective storms. Figure 3 also shows the breaking limit calculated using the Arctic observations[10] and the consequence of extrapolating small-amplitude wave theory to large-amplitude waves.

Motivated by our experimental results, we examine the wider relevance of wave breakup on sea-ice extent, proposing that an increase in significant wave height in the Southern Ocean would increase the breakup of sea ice, resulting in a retreat of the sea-ice edge. Conversely, for a decrease in significant wave height we would expect the ice edge to expand. To identify whether such a relationship exists, we compare model estimates of significant wave heights[19] with satellite sea-ice observations between 1997 and 2009, taking the 15% ice concentration contour to define the sea-ice edge. The data set was divided into two six-month seasons per year: growth (March to August) and decay (September to February) (Fig. 4). Both show that decreasing and increasing trends in sea-ice extent correlate with increasing and, respectively, decreasing trends in significant wave height (Pearson correlation coefficients were -0.70 in the decay season and -0.79 in the growth season). We find that a 2-m increase in significant wave height over a decade leads to a 2° latitudinal retreat in

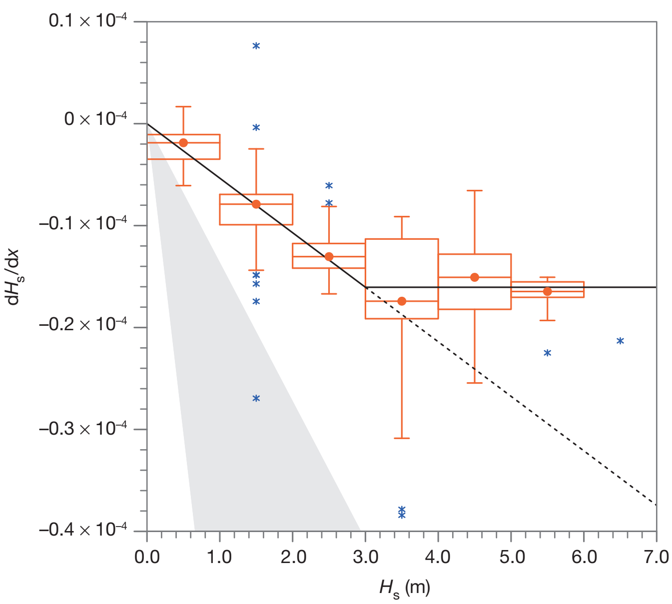

Figure 2 | Decay rates of sensors farther than 100 km from the ice edge. Data are binned in 1-m boxes. The red dot is the median. Box height shows the range within which 50% of the data lie. The whiskers give the range of data, excluding outliers (blue markers) and single data points. The solid black line is calculated from linear least-squares regression through the median values. The dashed black line shows the decay that would be expected if small-amplitude wave theory held for large waves. The grey region gives the range of decay rates observed in the Arctic[10].

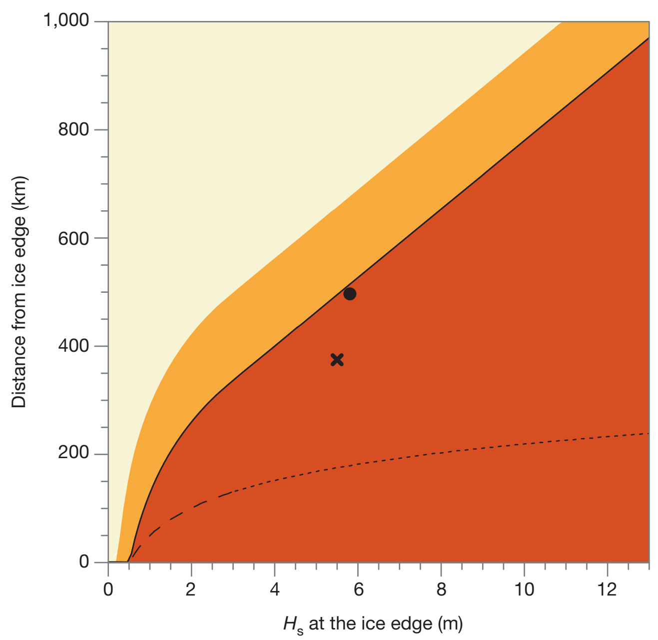

Figure 3 | Ice-breaking potential as a function of the distance from the ice edge and the significant wave height at the ice edge. Highlighted are conditions where breaking will not occur (yellow), may occur (orange) and is likely to occur (red). The long-dashed line is the likely breaking limit calculated using the attenuation coefficient observed in the Arctic[10] for small-amplitude waves with a 12-s period. This is extrapolated using small-amplitude wave theory (short-dashed). The markers show ice floe breakup events during this experiment at 11:00 on 1 October 2012 UTC (dot) and during a large-wave event in the Arctic[18] (cross).

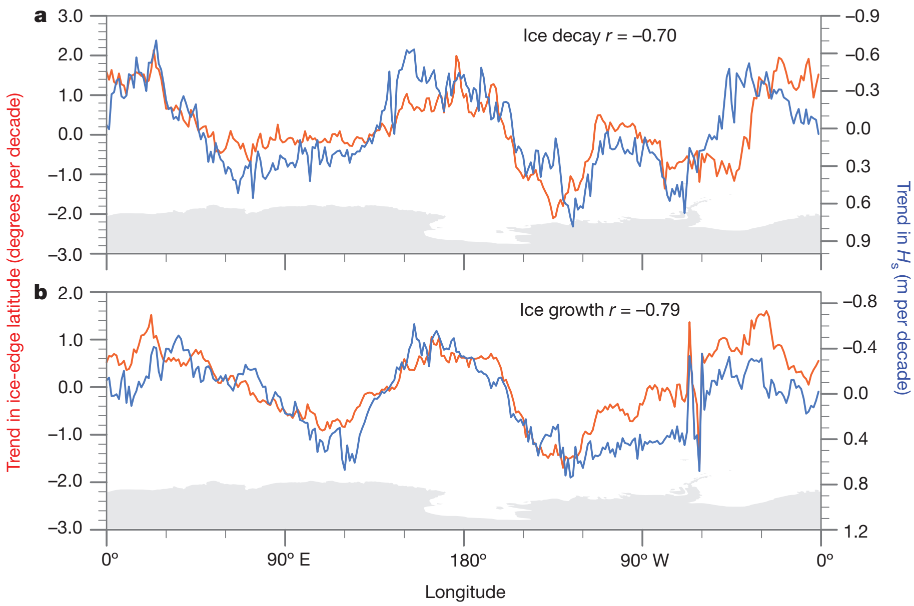

Figure 4 | A comparison between the trends in sea-ice extent and significant wave height between 1997 and 2009. The observed trend in the location of the ice edge (red) and the simulated trend in the significant wave height (blue) are shown as functions of longitude. **a**, Averaged trends for the ice decay season (September to February). **b**, The averaged trends during the ice growth season (March to August). The Pearson coefficient (r) is given at the top right of each panel ($n = 288$ for each). Antarctica is represented by the grey shaded region. We note that the scale for trend in H_s increases downwards.

ice extent (Extended Data Fig. 4). Spatially, the largest increases in wave height were found in the Amundsen–Bellingshausen Sea and the largest decreases were found in the Western Ross Sea (Fig. 4), areas where regional sea-ice retreat and expansion, respectively, are well documented[20]. The trends in significant wave height between 1997 and 2009 are consistent with the observed longer-term trends[11]. Identifying a similar relationship in the Arctic was not possible, owing to insufficient data.

Our results suggest that sea ice is vulnerable to changes in storminess. The observed southward shift in the storm tracks over recent decades has resulted in fewer cyclones at mid latitudes and more cyclones at higher latitudes[21]. However, the response has not been purely zonal; recent trends in the surface pressure pattern and winds have exhibited zonally asymmetric changes, resulting in variability in the atmospheric forcing of sea ice[22]. In the future, wave heights are predicted to increase everywhere at the sea-ice edge in the Arctic and Antarctic[23]. It is conceivable that this will act to accelerate sea-ice retreat.

Climate models continue to have difficulty in accurately predicting both Arctic sea-ice retreat and the regional variations in sea ice around Antarctica, suggesting either the inaccurate representation or the omission of important sea-ice physics. Our new observations show that slower decay by large waves ($>$3 m), possibly owing to nonlinear processes, allows waves to maintain ice-breaking potential hundreds of kilometres into the pack ice. This is a relationship that seems to be consistent around Antarctica, with changing wave heights correlating with changes in the latitude of the ice edge. This suggests that wave/sea-ice interactions need to be included in climate models, either directly or as parameterizations, before these models can improve their representations of sea ice. Although some sea-ice models are beginning to consider wave/sea-ice interactions, they may have limited success if they inadequately represent the behaviour of large storm-driven waves.

METHODS SUMMARY

The waves-in-ice observation system consisted of a high-resolution accelerometer coupled with a tri-axis inertial measurement unit (IMU), which was located using the Global Positioning System. Instruments simultaneously recorded wave accelerations for 34 min every 3 h. This record was filtered and integrated to calculate displacement, and a subsampled fast Fourier transform of the data was returned via satellite. Almost 600 data records were returned[24] (Extended Data Table 2). The data set is complex, owing to the significant spatial and temporal variation in wave forcing. To quantify how waves decay, we assume that the wave field is consistent along the zonal spread of the sensors, and that as waves enter the sea ice, they refract and travel south along a meridian. We compare only simultaneously collected instrument records, under the assumption that the wave climate persisted long enough to ensure that the wave spectra captured deep within the ice pack are from the wavefront captured near the ice edge. We further integrate the data by considering the decay of total wave energy, that is, the significant wave height, rather than the decay at individual frequencies. For each adjacent pair of sensors, we calculate the decay in significant wave height as a function of distance. The pairs are grouped into 1-m bins, determined by the significant wave height of the northernmost sensor. To take advantage of sea ice acting as a low-pass filter, we consider only pairs of sensors whose mean distance from the ice edge is greater than 100 km (Extended Data Table 3). Full details on our experiment design and analysis techniques are provided in Methods.

Online Content Any additional Methods, Extended Data display items and Source Data are available in the online version of the paper; references unique to these sections appear only in the online paper.

Received 23 December 2013; accepted 14 March 2014.

1. Wadhams, P. *Ice in the Ocean* 202–218 (Gordon and Breach, 2002).
2. Squire, V. A., Dugan, J. P., Wadhams, P., Rottier, P. J. & Liu, A. K. Of ocean waves and sea ice. *Annu. Rev. Fluid Mech.* **27,** 115–168 (1995).
3. Dumont, D., Kohout, A. & Bertino, L. A wave-based model for the marginal ice zone including a floe breaking parameterization. *J. Geophys. Res.* **116,** C04001 (2011).
4. Stroeve, J., Holland, M. M., Meier, W., Scambos, T. & Serreze, M. Arctic sea ice decline: faster than forecast. *Geophys. Res. Lett.* **34,** L09501 (2007).
5. Turner, J., Bracegirdle, T. J., Phillips, T., Marshall, G. J. & Hosking, J. S. An initial assessment of Antarctic sea ice extent in the CMIP5 models. *J. Clim.* **26,** 1473–1484 (2013).
6. Shackleton, E. H. *South: The Story of Shackleton's Last Expedition, 1914–17* 103 (Macmillan, 1982).
7. Kohout, A. L. & Meylan, M. H. An elastic plate model for wave attenuation and ice floe breaking in the marginal ice zone. *J. Geophys. Res.* **113,** C09016 (2008).
8. Williams, T. D., Bennetts, L. G., Squire, V. A., Dumont, D. & Bertino, L. Wave-ice interactions in the marginal ice zone. Part 2: numerical implementation and sensitivity studies along 1D transects of the ocean surface. *Ocean Model.* **71,** 92–101 (2013).
9. Wadhams, P., Squire, V. A., Goodman, D. J., Cowan, A. M. & Moore, S. C. The attenuation rates of ocean waves in the marginal ice zone. *J. Geophys. Res.* **93,** 6799–6818 (1988).
10. Squire, V. A. & Moore, S. C. Direct measurement of the attenuation of ocean waves by pack ice. *Nature* **283,** 365–368 (1980).
11. Young, I. R., Zeiger, S. & Babanin, A. V. Global trends in wind speed and wave height. *Science* **332,** 451–455 (2011).
12. Doble, M. J. & Bidlot, J.-R. Wave buoy measurements at the Antarctic sea ice edge compared with an enhanced ECMWF WAM: Progress towards global waves-in-ice modelling. *Ocean Model.* **70,** 166–173 (2013).

13. Marko, J. R. Observations and analyses of an intense waves-in-ice event in the Sea of Okhotsk. *J. Geophys. Res.* **108,** C9 (2003).
14. Squire, V. A. Of ocean waves and sea-ice revisited. *Cold Reg. Sci. Technol.* **49,** 110–133 (2007).
15. Longuet-Higgins, M. S. On the statistical distributions of sea waves. *J. Mar. Res.* **11,** 245–265 (1952).
16. Liu, A. K., Vachon, P. W., Peng, C. Y. & Bhogal, A. S. Wave attenuation in the marginal ice zone during LIMEX. *Atmos.-ocean* **30,** 192–206 (1992).
17. Komen, G. J. *et al. Dynamics and Modelling of Ocean Waves* 232 (Cambridge Univ. Press, 1994).
18. Prinsenberg, S. J. & Peterson, I. K. Observing regional-scale pack-ice decay processes with helicopter-borne sensors and moored upward-looking sonars. *Ann. Glaciol.* **52,** 35–42 (2011).
19. Chawla, A., Spindler, D. M. & Tolman, H. L. Validation of a thirty year wave hindcast using the Climate Forecast System Reanalysis winds. *Ocean Model.* **70,** 189–206 (2013).
20. Parkinson, C. L. & Cavalieri, D. J. Antarctic sea ice variability and trends, 1979–2010. *Cryosphere* **6,** 871–880 (2012).
21. Hartmann, D. L. *et al.* in *Climate Change 2013: The Physical Science Basis* (eds Stocker, F. F. *et al.*) 159–254 (Cambridge Univ. Press, 2013).
22. Holland, P. R. & Kwok, R. Wind-driven tends in Antarctic sea-ice drift. *Nature Geosci.* **5,** 872–875 (2012).
23. Dobrynin, M., Murawski, J. & Yang, S. Evolution of the global wind wave climate in CMIP5 experiments. *Geophys. Res. Lett.* **39,** L18606 (2012).
24. Kohout, A. L. & Williams, M. J. M. Waves-in-ice observations made during the SIPEX II voyage of the Aurora Australis, 2012. *Australian Antarctic Data Centre* http://dx.doi.org/10.4225/15/53266BEC9607F (2013).

Acknowledgements We thank Inprod Pty Ltd for instrument design and construction; M. Doble, V. Squire and T. Haskell for contributions toward instrument design; T. Toyota for the provision of ice floe size and ice thickness data; the captain and crew of RSV *Aurora Australis* and the second Sea Ice Physics and Ecosystem Experiment (SIPEX II) for their assistance in deploying the waves-in-ice instruments; and V. Squire, T. Toyota, L. Bennetts and T. Williams for contributions toward interpretation and editing. The work was funded by a New Zealand Foundation of Research Science and Technology Postdoctoral award to A.L.K.; the Marsden Fund Council, administered by the Royal Society of New Zealand; NIWA, through core funding under the National Climate Centre Climate Systems programme; the Antarctic Climate and Ecosystems Cooperative Research Centre; and Australian Antarctic Science project 4073.

Author Contributions A.L.K. and M.J.M.W. had the idea for and designed the study. A.L.K. carried out the experiment. A.L.K., S.M.D. and M.H.M. analysed the data. All authors contributed to data interpretation and writing.

Author Information Reprints and permissions information is available at www.nature.com/reprints. The authors declare no competing financial interests. Readers are welcome to comment on the online version of the paper. Correspondence and requests for materials should be addressed to A.L.K. (alison.kohout@niwa.co.nz).

METHODS

The waves-in-ice observation system. Five autonomous wave sensors were deployed during SIPEX II (the second Sea Ice Physics and Ecosystem Experiment) on Antarctic sea ice along a 250-km meridional transect[24]. These sensors simultaneously measured vertical acceleration and converted this to wave spectra. The spectra and sensor position were transmitted via the Iridium satellite system.

The waves-in-ice observation system consisted of a high-resolution Kistler ServoK-Beam accelerometer. To correct for vertical acceleration, each system also included a tri-axis IMU with an accelerometer, magnetometer and gyroscope. Positions were tracked using GPS.

Every 3 h, the instruments simultaneously became active and recorded wave accelerations for 34 min. Acceleration was sampled at 64 Hz and a low-pass, second-order Butterworth filter was applied with a cut-off at 2 s and subsampled to 0.5 s. A high-pass filter was then applied and the acceleration double-integrated to provide displacement. Welch's method, using a 10% cosine window and de-trending on four segments with 50% overlap, was applied to estimate the power spectral density[25].

The confidence interval for the power spectra is given by[26]

$$\left(\frac{\mathrm{PSD}(T)\times \mathrm{DoF}}{\chi^2(\mathrm{DoF},(1-\alpha)/2)},\frac{\mathrm{PSD}(T)\times \mathrm{DoF}}{\chi^2(\mathrm{DoF},(1+\alpha)/2)}\right)$$

where $\mathrm{PSD}(T)$ is the power spectral density as a function of period, χ^2 are percentage points of a chi-squared probability distribution and α defines the confidence interval; that is, $\alpha = 0.9$ provides a 90% confidence interval. DoF is the number of degrees of freedom. For a cosine window overlapping segmented data, the DoF can be approximated by[26]

$$\mathrm{DoF}\approx\frac{2K}{1+0.4(K-1)/K}$$

where K is the number of overlapping segments. Further variance reduction is achieved by averaging the harmonics once the record has been analysed[25]. If L bins are averaged together, DoF is increased by a factor of L. We reduce our 512 period bins to 55 period bins by averaging across five bins for periods less than 6 s, three bins for periods of 6–8 s, and five bins for periods greater than 20 s, with no averaging for periods of 8–20 s.

Because the Kistler accelerometer is inherently linear, each individual unit was tested at $\pm 1g$, obtaining specific offset and gain for each completed assembly. The IMU is factory calibrated. We found the differences between the two sensors were minimal for accelerations within the limit of the IMU. Each complete unit was tested down to $-20\,^{\circ}$C. The software and filtering processes were tested using a series of various pure sine waves, sine waves with artificially generated white noise, and acceleration time series from the Ross Sea MIZ[27]. The combined hardware and software was tested using a purpose-built calibration rig, which included a vertical slide driven by a connecting rod to a rotating wheel. The speed and amplitude of the wheel could be varied and we tested amplitudes between 3 and 20 cm, wave periods between 5 and 20 s and accelerations between $3\times10^{-5}g$ and $5\times10^{-2}g$. For periods greater than 20 s and amplitudes less than 32 mm, the test rig and component noise was too great to detect the wave source. As a final test, the sensors were deployed in a coastal environment to test measurement and analysis of real wave motion.

On 23 September 2012 UTC, three waves-in-ice observing systems were deployed from a hovering helicopter. These were deployed close to the ice edge and approximately 5 km apart (Fig. 1). Owing to a change in the weather, the remaining sensors were deployed using the RSV *Aurora Australis*'s aft crane. The sensor furthest from the ice edge (160 km) was deployed on 24 September 2012 (Fig. 1). The sensors were deployed on floes between 10 and 25 m wide and 0.5–1.0 m thick. These floes were small enough to follow the water surface for wavelengths greater than 100 m. Ice floes have an elastic response to waves and can bend and flex with the propagating waves, allowing the incident wave to propagate without significant interaction with the ice floe.

Each sensor generally drifted east, and slightly north, with the northernmost sensors drifting faster than the southernmost sensors. During the six-week recording period, the area covered by the sensors was bounded by 60° 30′ S–63° 0′ S and 120° 0′ E–129° 0′ E (Fig. 1). The sensors' survival depended on staying fixed to the floe. Each sensor dropped out either during a storm or if they travelled too far beyond the ice edge. In either case, the floe presumably melted or the sensor was washed off in rough seas.

Ice floe characteristics. During deployment, the floe size distribution was monitored using a camera installed on the upper deck of the ship[28]. A digital image was captured every minute. Analysis of these ship-borne images is shown in Extended Data Table 1. The Antarctic MIZ in the region where the instruments were deployed consisted of first-year ice on average 0.75 m thick. We define the ice edge as the line of 15% ice concentration determined using the ASI algorithm SSMI-SSMIS sea-ice concentrations[29–31].

Analysis. Quality control is maintained by returning the number of spikes, flat spots, the gyro standard deviation and a 55-bin wave spectrum. Spikes are defined if a measurement is greater than 6 s.d. from the mean. According to Chebyshev's inequality, for all distributions at least 97% of the data will be within 6 s.d. of the mean. Spikes and flat spots are linearly interpolated in time from the adjoining valid points. Extended Data Table 2 shows the percentage of missing values for each sensor.

The spectral moments are also returned and the significant wave height was calculated from the zeroth spectral moment, defining the total variance (or energy) of the wave system. The confidence interval for H_s is approximately -10% to $+15\%$ (ref. 26). For each sampling period, the maximum and minimum longitudes of the five sensors are found. For each longitude in the range, the latitude is found where the ice concentration is first greater than 15%. We then average across the longitudes to find the mean ice extent for each record. The distance from the ice edge of each sensor is then calculated using only the sensor's latitude. This minimizes the distance we assume the wave has travelled from the ice edge.

Having defined the distance from the ice edge, we can consider the decay in wave height as a function of distance, assuming that the wave field is consistent along the zonal spread of the sensors and that as waves enter the sea ice they refract and travel meridionally south. We also assume that for each record the wave climate persisted long enough to ensure that the wave spectra captured deep within the ice pack is from the wavefront captured near the ice edge. We calculate the decay for each adjoining pair of sensors and present this using a box plot because it is non-parametric and its characterization of the distribution is resilient to outliers. The northernmost sensor determines which wave height bin the data point fits into (Extended Data Table 3). Each bin is sorted and the median, twenty-fifth percentile and seventy-fifth percentile are calculated. Outliers are allocated if they are beyond $1.5\times$ IQR, where IQR is the interquartile range. To take advantage of sea ice acting as a low-pass filter, we consider only the median decay rate in each bin whose mean distance from the ice edge is greater than 100 km, we calculate a line of best fit to the decay rates as a function of significant wave height (equation (1)).

Direct observation of waves near the ice edge clearly shows that waves are a complex combination of interacting waves with significant variation in amplitude and wave period. Away from the ice edge, the ice dampens the waves. For this reason, we focus our attention on observations more than 100 km from the ice edge. Although there is more noise within 100 km of open water, the $\mathrm{d}H_s/\mathrm{d}x$ relationship is equally robust (Extended Data Table 3).

Strain is related to the ice thickness and wave displacement by

$$S=\frac{h}{2}\frac{\partial^2\eta}{\partial x^2}$$

where h is the ice thickness, x is the propagating distance and η is the displacement[7]. Assuming that $\eta(x,t)=H\mathrm{e}^{i(kx-\omega t)}/2$, where H is the wave height at a single frequency with wavenumber k and frequency ω, we find that

$$S=\frac{1}{4}k^2hH=\frac{(2\pi)^4hH}{4T^4g^2} \qquad (2)$$

where T is the wave period and g is the acceleration due to gravity. Given equation (2), if we know the strain failure, the peak period and floe thickness, we can approximate the wave height at which the floes will break due to strain. Hence, given a wave height at the ice edge, we use equation (1) to approximate the wave height as a function of distance. Using equation (2), we can then approximate for a given wave at the ice edge, the distance into the ice edge where the wave height will no longer be sufficient to break floes (Fig. 3).

The trend in sea ice extent versus wave height. For the period 1997–2009, we use the NOAA/NSIDC Climate Data Record of Passive Microwave Sea Ice Concentrations[32,33] and the NOAA WAVEWATCH III CFSR Reanalysis Hindcast[19] to calculate the trend in sea-ice extent relative to the trend in significant wave height for each longitude. For each longitude, the sea-ice extent is defined as the latitude at which the 15% ice concentration is first reached. The maximum extent plus 2° to the north provides the latitude for which the corresponding wave heights are given. This ensures wave heights are consistent across the years and are not influenced by proximity to the ice edge. Trends in sea-ice extent and wave height are then calculated for each longitude. Pearson correlation coefficients are provided for the averaged trends for each longitude (Fig. 4) and for the full monthly data set (Extended Data Fig. 4). An analysis of the residuals in the regression for the monthly data suggests that only the central part of the residuals is normally distributed.

25. Tucker, M. J. & Pitt, E. G. *Waves in Ocean Engineering* (Elsevier, 2001).
26. Earle, M. D. *Nondirectional and Directional Wave Data Analysis Procedures*. NDBC Technical Document 96-01 (US Department of Commerce, 1996).
27. Downer, J. & Haskell, T. G. Ice-floe kinematics in the Ross Sea marginal ice zone using GPS and accelerometers. *Ann. Glaciol.* **33,** 345–349 (2001).
28. Toyota, T., Takatsuji, S. & Nakayama, M. Characteristics of sea ice floe size distribution in the seasonal ice zone. *Geophys. Res. Lett.* **33,** L02616 (2006).

29. Kaleschke, L. & Kern, S. Sea-ice concentration for Arctic & Antarctic (ASI-SSMI). *Integrated Data Climate Center* http:/icdc.zmaw.de/seaiceconcentration_asi_ssmi.html (2006).
30. Kaleschke, L. *et al.* SSM/I sea ice remote sensing for mesoscale ocean-atmosphere interaction analysis. *Can. J. Rem. Sens.* **27,** 526–537 (2001).
31. Spreen, G., Kaleschke, L. & Heygster, G. Sea ice remote sensing using AMSR-E GHz Channels. *J. Geophys. Res.* **113,** C02S03 (2008).
32. Meier, W. *et al.* NOAA/NSIDC *Climate Data Record of Passive Microwave Sea Ice Concentration* Version 2 (National Snow and Ice Data Center, Boulder, 2013); http://dx.doi.org/10.7265/N55M63M1.
33. Peng, G., Meier, W., Scott, D. & Savoie, M. A long-term and reproducible passive microwave sea ice concentration data record for climate studies and monitoring. *Earth Syst. Sci. Data* **5,** 311–318 (2013).
34. Dee, D. P. *et al.* The ERA-Interim reanalysis: configuration and performance of the data assimilation system. *Q. J. R. Meteorol. Soc.* **137,** 553–597 (2011).

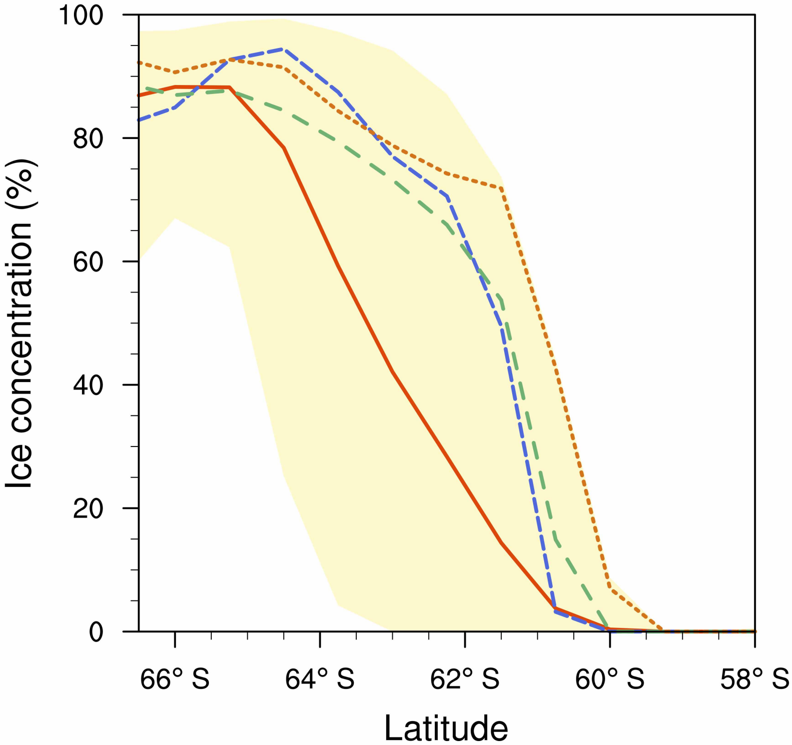

Extended Data Figure 1 | Latitudinal profiles of sea-ice concentration. ERA-Interim reanalysis of satellite observations[34] is averaged between 120° E and 129° E for the peak of each large-wave event: 23 September 2012 at 18:00 (blue long-dashed), 1 October 2013 at 12:00 (green long-dashed) and 7 October 2012 at 12:00 (orange short-dashed) (all dates in UTC). The solid line is the mean concentration (120 °E–129° E) between 15 September and 15 October for 1979–2012, and the shaded area (yellow) spans the maximum and minimum concentrations over the same time period.

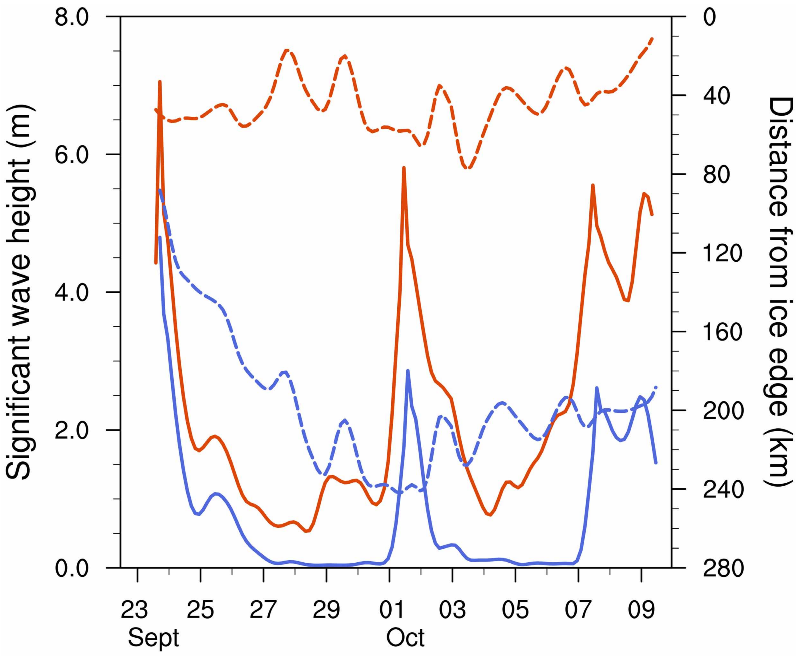

Extended Data Figure 2 | Overview of the observations. Smoothed significant wave height (solid) and smoothed distance from the ice edge (dashed) of the sensor closest to the ice edge (red) and the sensor farthest from the ice edge (blue). The ice edge is derived from the ASI algorithm SSMI-SSMIS sea-ice concentrations[29–31]. Dates are in UTC.

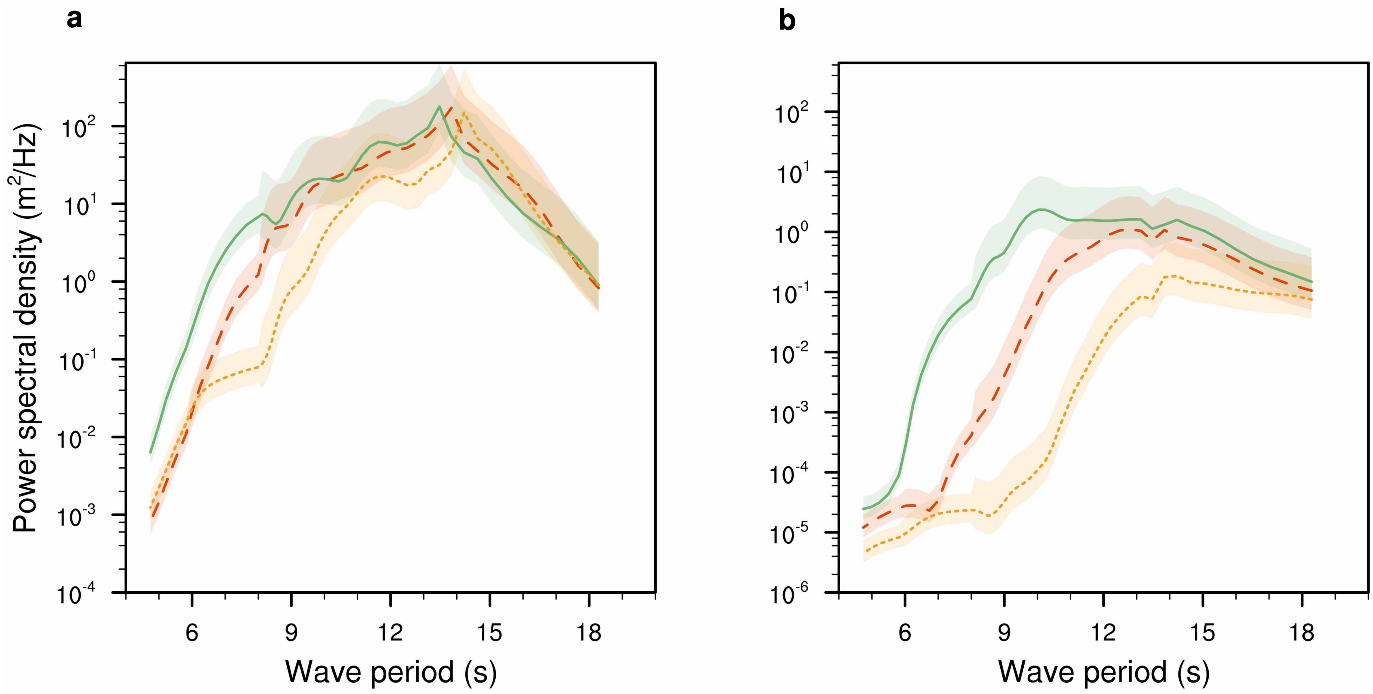

Extended Data Figure 3 | The power spectral densities during a storm-generated wave event and during calm seas. a, A storm-generated wave event at 20:00 on 23 September 2012 UTC with significant wave heights of 6, 5.5 and 4.2 m at, respectively, 39 (green solid), 51 (red dashed) and 90 km (yellow dotted) from the ice edge. **b**, Calm conditions at 02:00 on 27 September 2012 UTC with significant wave heights of 2, 1.3 and 0.1 m at, respectively, 0 (green solid), 14 (red dashed) and 150 km (yellow dotted) from the ice edge. The shaded regions give the 90% confidence intervals.

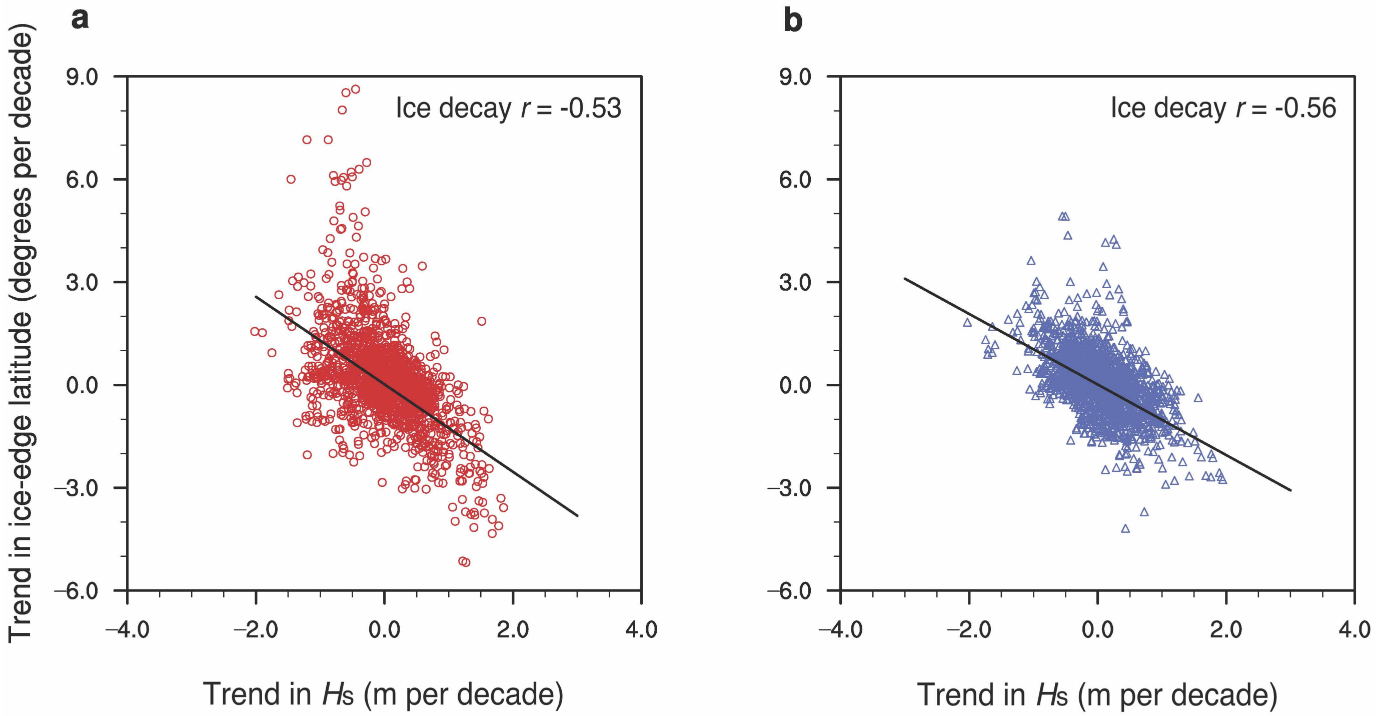

Extended Data Figure 4 | Trend in the location of the ice edge versus trend in significant wave height for each longitude and each month between 1997 and 2009. **a**, The trends during the ice decay season (September to February). **b**, The trends during the ice growth season (March to August). The Pearson coefficients are given in the top right of each panel (n = 1,727 for each). The linear least-squares approximation during ice decay is −1.28 (H_s trend) + 0.02, with a 95% confidence interval of (−1.39, −1.16) for the slope. During ice growth, it is −1.03 (H_s trend) + 0.01, with a 95% confidence interval of (−1.12, −0.94) for the slope.

Extended Data Table 1 | Floe size distribution

Location (decimal degrees south)	Dominant floe size (m)
61.0° – 61.6°	2 – 3
61.6° – 61.9°	5 – 6
61.9° – 62.7°	10 – 20
62.7° –	> 100

Extended Data Table 2 | Numbers of data points and missing values for each sensor

Sensor	Total no. of data points	No. of missing values (%)
1	133	1.5
2	73	4.1
3	72	0.0
4	7	42.9
5	313	0.3

Extended Data Table 3 | A comparison of dH_s/dx values for the full data set and for data more than 100 km from the ice edge

H_s (m)	No. of pairs		Median ($\times 10^{-4}$)		IQR ($\times 10^{-4}$)	
	All	> 100 km	All	> 100 km	All	> 100 km
0 - 1	84	57	-0.031	-0.019	0.040	0.024
1 - 2	97	38	-0.089	-0.079	0.081	0.030
2 - 3	31	21	-0.130	-0.130	0.050	0.024
3 - 4	16	11	-0.175	-0.174	0.189	0.078
4 - 5	25	14	-0.190	-0.151	0.131	0.054
5 – 6	10	5	-0.198	-0.165	0.078	0.015
6 – 7	4	1	-0.331	-	1.490	-
7 - 8	1	0	-	-	-	-

The median and interquartile range are given for the set of dH_s/dx values within each bin of significant wave heights.